Torus fractalization and intermittency

Sergey P. Kuznetsov
Institute of Radio-Electronics, Russian Academy of Sciences, Zelenaya 38, Saratov 410019, Russian Federation
(Received 19 December 2001; published 24 June 2002)

The bifurcation transition is studied for the onset of intermittency analogous to the Pomeau-Manneville mechanism of type I, but generalized for the presence of a quasiperiodic external force. The analysis is concentrated on the torus-fractalization (TF) critical point that occurs at some critical amplitude of driving. (At smaller amplitudes the bifurcation corresponds to a collision and subsequent disappearance of two smooth invariant curves, and at larger amplitudes it is a touch of attractor and repeller at some fractal set without coincidence.) For the TF critical point, renormalization group (RG) analysis is developed. For the golden mean rotation number a nontrivial fixed-point solution of the RG equation is found in a class of fractional-linear functions with coefficients depending on the phase variable. Universal constants are computed that are responsible for scaling in phase space ($\alpha = 2.890\,053\ldots$ and $\beta = -1.618\,034\ldots$) and in parameter space ($\delta_1 = 3.134\,272\ldots$ and $\delta_2 = 1.618\,034\ldots$). An analogy with the Harper equation is outlined, which reveals important peculiarities of the transition. For amplitudes of driving less than the critical value the transition leads (in the presence of an appropriate reinjection mechanism) to intermittent chaotic regimes; in the supercritical case it gives rise to a strange nonchaotic attractor.

DOI: 10.1103/PhysRevE.65.066209 PACS number(s): 05.45.Df, 05.10.Cc

I. INTRODUCTION

It is commonly believed that under parameter variation the turbulent dynamics in multidimensional systems may arise via quasiperiodicity, in the course of subsequent creation of oscillatory components with incommensurate frequencies, followed by chaotization (see, e.g., the works of Landau, Hopf, and Ruelle and Takens [1–3]).

Now it is well known that the actual details of the transition from quasiperiodicity to chaos are very subtle and complicated. Some of them can be revealed if we turn to a kind of restricted problem: Suppose that the system can be decomposed to a master subsystem with quasiperiodic behavior and a driven slave subsystem, and the latter can demonstrate transition to chaos. So, we may ask, what are possible scenarios for the onset of chaos in the second subsystem? (Note the analogy with the approach to the problem of three bodies in celestial mechanics: Although difficult in a general formulation, it allows an essential advance in a restricted version, under the suggestion that one of the bodies is of negligible mass.) One of the important results from this line of reasoning was a formulation of the concept of a strange nonchaotic attractor (SNA), which typically appears in an intermediate region between order and chaos [4–6]. In the phase space this is an object of fractal geometrical structure, but without instability with respect to the initial conditions in the driven system.

One more essential idea consists in the application of the renormalization group (RG) approach, proven to be very efficient for understanding dynamics in critical states between order and chaos (e.g., [7–16]). Starting with an evolution operator for some definite time interval we are able to construct the evolution operator for a larger interval. Then, we try to produce an appropriate variable change to make the new operator as close as possible to the original. This is just one step of the RG transformation, and it may be repeated again and again to obtain operators for larger and larger time intervals. As a result, we arrive at some universal operator, which describes the long-time evolution of the system at criticality. It is often represented by a fixed point of the RG transformation. Studies of this fixed-point operator together with consideration of its relevant perturbations reveal properties of universality and scaling for the transition. Originally, this approach was developed by Feigenbaum for the period-doubling scenario of the onset of chaos [7,8]; afterward it was applied to many other situations, including quasiperiodicity at the chaos border [10–12] and some cases of the creation of SNA [14–16].

Finally, we have to mention here a concept of intermittency suggested by Pomeau and Manneville [17]. It occurs in very general circumstances near a saddle-node bifurcation [also called a tangent bifurcation, preferably in the context of one-dimensional (1D) maps]. It was studied in different aspects by many authors. In particular, the RG approach was applied to intermittency in Refs. [18,19].

The goal of the present article is to consider a generalization of the Pomeau-Manneville mechanism for the case of the presence of quasiperiodic driving, and to reveal details of the bifurcation transition, which is an analog of the tangent bifurcation in this case. It is natural to regard the situation as one possible scenario of transition from quasiperiodicity to chaos in the context of the mentioned ''restricted problem.'' At small amplitudes of driving, the transition is rather trivial and consists in collision with coincidence (and subsequent disappearance) of a pair of smooth stable and unstable tori; see, e.g., [20,21]. However, at a definite value of the amplitude a nontrivial critical situation occurs. It allows application of the RG approach that will be developed. Also, the associated scaling properties will be revealed and discussed.

In Sec. II we introduce the basic model map and review its dynamical phenomena in the presence of the external quasiperiodic driving. In Sec. III we consider some details of dynamics in terms of rational approximations of the frequency parameter and locate numerically the critical point

associated with the threshold of fractalization at the moment of collision of the invariant curves. In Sec. IV we discuss the link between the problem under study and the Harper equation—the lattice version of the one-dimensional Schrödinger equation, well known in the context of solid-state physics [22–27]. In Sec. V the RG analysis is developed for the situation of tori fractalization: The RG equation is derived, and results of its numerical solution are presented. In Sec. VI we discuss scaling properties of the dynamics at the critical point. In Sec. VII the linearized RG equation is derived, the spectrum of eigenvalues is obtained, and two relevant eigenvalues responsible for scaling in the parameter plane are distinguished. In Sec. VIII we consider the consequences of these results concerning dynamics in a neighborhood of the critical point in the parameter space. In particular, we extract from the RG results the critical exponents for the duration of the laminar stages of intermittency and compare them with empirical numerical data. In conclusion, we discuss some perspectives of further studies in the context of the general problem of understanding the transition from the usual quasiperiodic regimes (''smooth torus'') to SNA and chaos.

II. THE MODEL AND BASIC PHENOMENA

Let us start with an example of a quasiperiodically forced 1D map

$$x_{n+1}=f(x_n)+b+\epsilon\cos 2\pi n w, \tag{1}$$

where ϵ and w are the amplitude and frequency parameters of the external force, respectively. We assume that the frequency parameter, also called the rotation number, is taken to be equal to the inverse golden mean $w=(\sqrt{5}-1)/2$. As to the function $f(x)$, let us define it here as

$$f(x)=\begin{cases} x/(1-x), & x\leqslant 0.75, \\ 9/2x-3, & x>0.75. \end{cases} \tag{2}$$

[One branch of the mapping is selected in the form of the fractional-linear function $x/(1-x)$, which appears naturally in the analysis of dynamics near the tangent bifurcation associated with intermittency; see, e.g., [18,19]. The other branch is attached somewhat arbitrarily to ensure presence of the reinjection mechanism in the dynamics.]

At zero amplitude of driving what we have is the usual transition to chaos via the Pomeau-Manneville intermittency of type I, controlled by the parameter b [see Fig. 1(a)]. At $b<0$ the map has two fixed points on the left branch, one stable and one unstable. Under increase of b these points approach one another, collide, and then disappear. After that, at $b>0$, a narrow ''channel'' remains at the place of former existence of the pair of fixed points, and travel across this channel is a slow process—the laminar stage of intermittency. Closer to the bifurcation point $b=0$, a larger number of iterations is required to pass the channel. After visiting the right-hand branch (the turbulent stage of the intermittency) the orbit quickly returns to the left, and travels through the channel again and again.

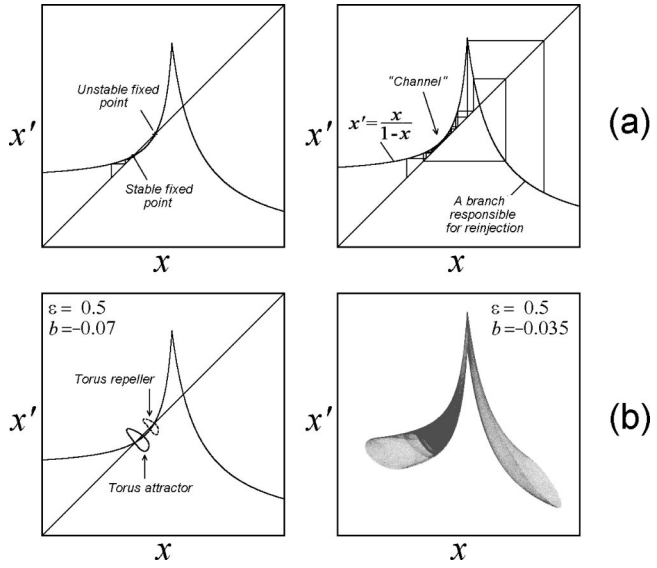

FIG. 1. Onset of chaos via the Pomeau-Manneville intermittency of type I in the model map (1) at $\epsilon=0$ (a), and the transition via collision and disappearance of smooth closed invariant curves, attractor and repeller (b). The diagrams are shown in the plane (x,x'), where x' relates to the moment of time one unit later than x. The left panels correspond to the situation before the bifurcation, and the right panels to the situation after the transition.

If the amplitude of driving is finite (although sufficiently small), then instead of the fixed points we observe a pair of closed smooth invariant curves, attractor and repeller [see Fig. 1(b)]. (A closed invariant curve may be thought of as a cross section of a torus. For brevity, it is convenient sometimes to speak about stable and unstable tori rather than about the invariant curves.) With increase of b, the attractor and repeller come nearer to each other and collide, and the localized attractor-repeller pair disappears. After that an extended attractor arises of a form shown in the right panel of Fig. 1(b). On the diagram the degree of darkness reflects the relative duration of the presence of the orbit in different parts of the attractor.

While we remain close to the point of bifurcation, the laminar stages of dynamics may be distinguished, which occupy an overwhelming part of the observation time, as in the case of the usual Pomeau-Manneville intermittency. In Fig. 1(b) they correspond to the domain of the most long-living residence—along the left branch of the map, at the place of location of the former attractor-repeller pair. In our study we will concentrate on the analysis of the laminar stages in the same way as is commonly accepted in the case of conventional intermittency. For this, it is sufficient to use the map

$$x_{n+1}=x_n/(1-x_n)+b+\epsilon\cos(2\pi n w). \tag{3}$$

As the numerical simulations clearly demonstrate, the collision of the attractor-repeller pair is of a different nature at small and at large amplitudes of driving. Similar observations were reported earlier in computations for the driven circle map [21,28].

At ϵ less than some critical value ϵ_c (in our map $\epsilon_c=2$) we observe that the invariant curves remain smooth until the

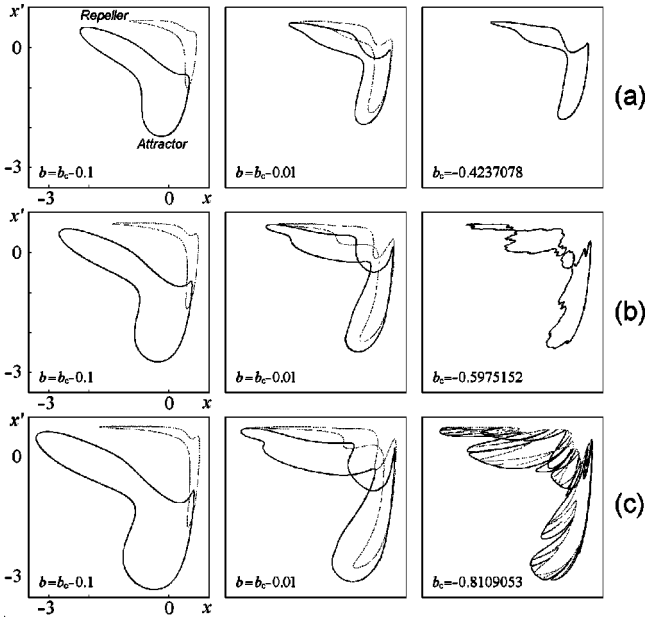

FIG. 2. Bifurcation of collision of the closed invariant curves in subcritical (a), critical (b), and supercritical (c) situations, at $\epsilon = 1.7$, 2, and 2.3, respectively. The invariant curves representing the attractor are shown by solid lines, and those for the repeller by dashed. The parameter b grows from left to right, and the last panel in a row corresponds to the moment of collision.

collision, and they precisely coincide with one another at that moment [Fig. 2(a)]. For $\epsilon = \epsilon_c$ they also coincide at the collision, but here the form of the invariant curve appears to be wrinkled [Fig. 2(b)]. Finally, at $\epsilon > \epsilon_c$, one can see that the collision takes place only at some fractal subset of points on the invariant curves, and no coincidence of the entire curves is observed [Fig. 2(c)].

The essential change in the nature of the transition with passage from $\epsilon < \epsilon_c$ to $\epsilon > \epsilon_c$ may be demonstrated also by computations of the Lyapunov exponent. Figure 3(a) shows the behavior of the Lyapunov exponent along the bifurcation border (at the collision of the attractor-repeller pair) as a function of the amplitude of driving. Observe that for $\epsilon < \epsilon_c$ the Lyapunov exponent has constant zero value, but for $\epsilon > \epsilon_c$ it becomes negative and decreases with growth of ϵ according to a visually perfect linear law. Figure 3(b) depicts a diagram for the Lyapunov exponent dependence on b at

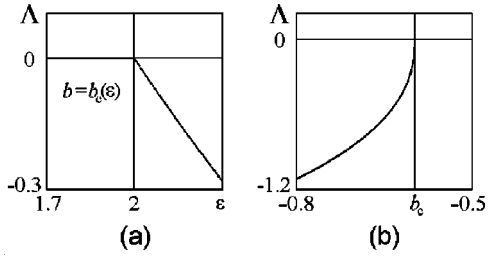

FIG. 3. The Lyapunov exponent at the bifurcation border versus the amplitude parameter ϵ (a) and dependence of the Lyapunov exponent on the parameter b at critical $\epsilon = 2$ (b) for the fractional-linear map with quasiperiodic driving.

TABLE I. The values of b for the first attractor-repeller collision at the critical amplitude $\varepsilon = 2$.

w_k	b
8/13	-0.5989496730498198
13/21	-0.5993564164969890
21/34	-0.5975700101088623
34/55	-0.5977371349948819
55/89	-0.5975077597293093
89/144	-0.5975427315192966
144/233	-0.5975125430279679
233/377	-0.5975187094612125
377/610	-0.5975146415227064
610/987	-0.5975156490874847
987/1597	-0.5975150899217102
1597/2584	-0.5975152478940331
2584/4181	-0.5975151698106684
4181/6765	-0.5975151939749183
6765/10946	-0.5975151829388339
10946/17711	-0.5975151865779841

fixed $\epsilon = \epsilon_c$; it shows essentially distinct behavior; apparently a power law with a nontrivial exponent.

The intriguing fact that the change of character of the bifurcation in the model map (3) takes place precisely at $\epsilon_c = 2$ will be explained in Sec. IV.

III. METHOD OF RATIONAL APPROXIMATIONS

As is well known, the irrational $w = (\sqrt{5}-1)/2$ taken as the frequency parameter in the driven map is a limit of a sequence of rationals $w_k = F_{k-1}/F_k$, where F_k are the Fibonacci numbers ($F_0 = 0$, $F_1 = 1$, $F_{k+1} = F_k + F_{k-1}$). Let us change the rotational number w to its approximant w_k, and introduce a parameter of initial phase u into the equation:

$$x_{n+1} = x_n/(1-x_n) + b + \epsilon \cos 2\pi(nw_k + u). \qquad (4)$$

Now, below the transition, at any fixed u we have a pair of cycles of period F_k, one stable and the other unstable. The Floquet eigenvalue, or multiplier μ, which characterizes the decrease of a perturbation over one period of the stable cycle, will depend on u. This dependence appears to be periodic, with period $2\pi/F_k$. For a given ϵ we may select numerically such b that the maximal value of μ at some phase reaches 1, and μ is less than 1 at other phases. It corresponds just to the first tangent bifurcation, that is, a collision of the earlier stable cycle of period F_k with its unstable partner. Technically, the computations are simplified by two observations: first, the maximum of the multiplier occurs at $u = 0$, and, second, the initial condition for the cycle at the situation of collision may be expressed explicitly [see Eq. (16) in Sec. IV].

In Table I we present numerical data for the values of b corresponding to the cycle collision at $u = 0$ for the critical amplitude $\epsilon = 2$. Figure 4 shows the multiplier as a function

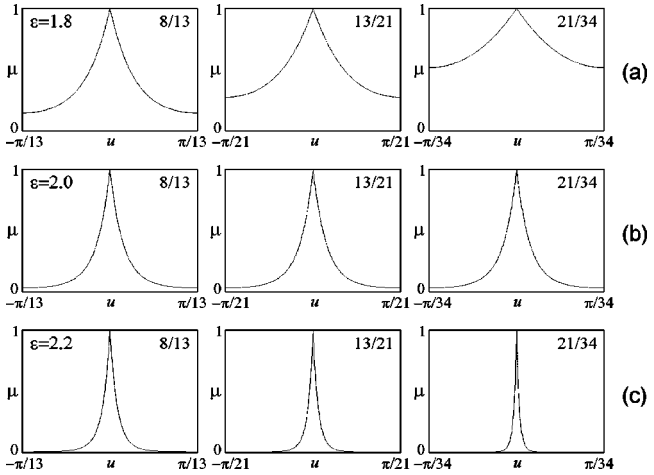

FIG. 4. Floquet eigenvalue or multiplier μ computed at three subsequent levels of rational approximation versus phase variable u at the values of b corresponding to the moments of the first cycle collision for subcritical (a), critical (b), and supercritical (c) amplitudes.

of the phase u in an interval of periodicity at the moment of the first tangent bifurcation. The diagrams are plotted at three subsequent levels of the rational approximation for the amplitude parameter less than, equal to, and larger than 2.

For $\epsilon<2$ the dependencies become more flat under increase of the order of the rational approximation (the bifurcation tends to become ''phase independent''). In contrast, for $\epsilon>2$ the curves tend to become sharper. At $\epsilon=2$ the form of the curves looks to be stabilized at subsequent levels of the rational approximation.

It is interesting to discuss the relation of these observations with the behavior of the Lyapunov exponent at the transition. As we consider the attractor for the irrational rotation number in terms of a certain rational approxinmant $w_k=F_{k-1}/F_k$, it looks like a collection (continuum set) of periodic orbits, each of which is associated with a particular initial phase u and has a value the of Lyapunov exponent $\Lambda(u)=(1/F_k)\ln\mu(u)$. To obtain in this approximation an estimate for the Lyapunov exponent of the whole attractor, we have to perform averaging over the initial phases, $\Lambda=\langle\Lambda(u)\rangle$. From the behavior of the multipliers in the subcritical case we conclude that the value of Λ will tend to zero under increase of the order of rational approximation. In the supercritical case only a very pure subset of the orbits will have multipliers distant from 0 and close to 1, so the average value of Λ is negative. These arguments are in agreement with the observed dependence of the Lyapunov exponent on the parameter b along the bifurcation curve [see the previous section, Fig. 3(a)].

As seen from Table I, the bifurcation sequence converges to a well-defined limit

$$b=b_c=-0.597\,515\,185\,376\,121\ldots \tag{5}$$

(see also a remark in the final part of Sec. VI). It is a numerical estimate for the parameter value associated with the critical point of fractalization of the colliding tori. It will be referred to as the torus-fractalization (TF) critical point. The dynamics at this point and in its vicinity is the main subject of our study in Sec. V and further.

IV. A LINK WITH THE HARPER EQUATION

The Schrödinger equation in normalized form for a quantum particle in a one-dimensional discrete lattice with additional quasiperiodic potential reads

$$i\frac{\partial\psi_n}{\partial t}=\psi_{n+1}+\psi_{n-1}-2\psi_n+(\epsilon\cos 2\pi nw)\psi_n, \tag{6}$$

where n is the spatial index, ϵ is the amplitude of the quasiperiodic potential, and w defines its wave number. Alternatively, one can speak of a wave process in a lattice medium with supplied sustained quasiperiodic perturbation. For an oscillatory solution of frequency Ω (which corresponds to a state of the quantum particle of definite energy) the exponential substitution $\psi_n\propto\exp(i\Omega t)$ yields

$$\psi_{n+1}+\psi_{n-1}-2\psi_n+(\Omega+\epsilon\cos 2\pi nw)\psi_n=0. \tag{7}$$

This is the so-called Harper equation well known in the context of solid-state physics [22–27].

Let us return to our fractional-linear map (3) and perform the variable change

$$x_n=1-\psi_n/\psi_{n-1}. \tag{8}$$

The result is exactly the Harper equation (7) with Ω changed to b:

$$\psi_{n+1}+\psi_{n-1}-2\psi_n+(b+\epsilon\cos 2\pi nw)\psi_n=0. \tag{9}$$

The link between the Harper equation and the fractional-linear mappings was noticed and exploited earlier by Ketoja and Satija [25], although they were interested in different problems than that of our concern here. Recently, the same idea was effectively used for analysis of spectral properties of the Harper equation in Ref. [27].

At rational approximants of the wave number w the expression (7) becomes an equation with periodic coefficients. Together with the Floquet condition

$$\psi_{n+q}=\mu\psi_n=\psi_n e^{i\tilde{\beta}q},$$

$$\tilde{\beta}=(\arg\mu+2\pi m)/q,\quad q=F_k, \tag{10}$$

it gives rise to an eigenvalue problem: At any given wave number $\tilde{\beta}$ one can obtain (say, numerically [24]) a spectrum of frequencies

$$\Omega=\Omega(\tilde{\beta}). \tag{11}$$

It is called a dispersion equation for the waves in the medium governed by Eq. (6). If the equation has a real root $\tilde{\beta}$ at a given Ω, it corresponds to wave propagation, or a transmission band. If the equation has no real but only complex solutions, we say that Ω is in a forbidden zone, or in a non-

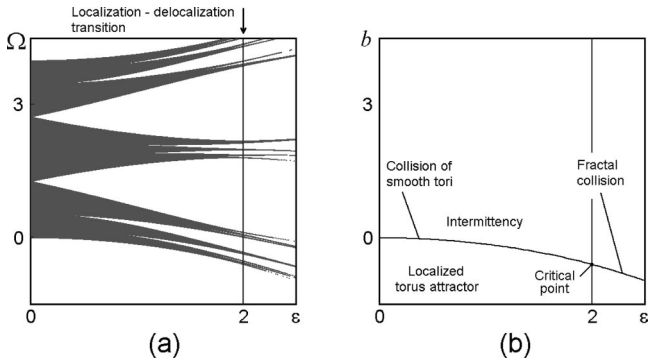

FIG. 5. Transmission bands (gray) and forbidden zones (white) in the parameter plane (ϵ,Ω) for the Harper equation (a), and the chart of dynamical regimes (phase diagram) for intermittency under quasiperiodic driving (b). The bifurcation curve of the attractor-repeller collision in the panel (b) exactly corresponds to the bottom border of the gray area in the diagram (a).

transmission band. In this case there are no propagating waves, but spatial exponential decay occurs at the given frequency.

To understand the relation between the nature of solutions of the Harper equation and those of our original problem, let us turn to a particular case of slow spatial variation of ψ_n, use the continuous limit, and set $\epsilon=0$. That yields

$$\Psi''+b\Psi=0. \tag{12}$$

Now, at $b<0$ we have solutions of the form $\Psi_n=C\exp(\pm\sqrt{|b|}n)$, and, according to Eq. (12), $x_n=1-\psi_n/\psi_{n-1}=1-\exp(\pm\sqrt{|b|})$. It corresponds to the presence of two fixed points. At $b>0$ we obtain $\Psi_n=C\cos(\sqrt{b}n)$. Then, $x_n=1-\psi_n/\psi_{n-1}\to\infty$ as $n\to\pi/(2\sqrt{b})$; this means that no localized attractor is present. In the same manner, a forbidden zone of the Harper equation must be associated with the existence of a localized attractor-repeller pair of the driven fractional-linear map, while a transmission band corresponds to the presence of the ''channel'' and to the laminar stages of intermittency (see also [27]).

It is easy to find that for $\epsilon=0$ the transmission band in the Harper model occupies an interval of Ω from 0 to 4. At nonzero ϵ the forbidden zones (''gaps'') arise inside the band, and they become wider as ϵ grows. Under increase of the order of rational approximation k, new and narrower gaps appear inside the transmission bands. For $\epsilon<2$ in the limit $k\to\infty$ the transmission bands of higher orders dominate over the forbidden zones (i.e., they have a larger total width), but for $\epsilon>2$ the situation is opposite [23,24]. The transition from one type of behavior to another is known as the localization-delocalization transition. The structure of the transmission bands at the transition appears to be a kind of Cantor-like set. Figure 5(a) shows the transmission and forbidden zones colored, respectively, gray and white in the parameter plane (ϵ,Ω).

The fact that the transition in the Harper equation must take place at $\epsilon=2$ follows from the argument of Aubry [29,24]. By means of the Fourier-like transformation

$$\phi_k=\hat{F}\psi_n=\sum_{n=-\infty}^{\infty}\psi_n e^{2\pi ink w} \tag{13}$$

one obtains from Eq. (7) an equation of similar form,

$$\phi_{k+1}+\phi_{k-1}-2\phi_k+[\Omega'+\epsilon'\cos(2\pi ikw)]\phi_k=0, \tag{14}$$

but with parameters

$$\Omega'=2+2(\Omega-2)/\epsilon,\quad \epsilon'=4/\epsilon. \tag{15}$$

Localization of a wave function implies delocalization of its transform, and vice versa. So the transition has to occur at $\epsilon=2$, which corresponds to a fixed point of the equation for ϵ.

In Fig. 5(a) one can find a forbidden zone in the bottom part of the diagram. Obviously, its top border must correspond to the threshold of intermittency in the fractional-linear map. As may be observed from comparison of Figs. 5(a) and 5(b), this is indeed the case. The TF critical point found in the previous section corresponds exactly to the lowest frequency associated with the appearance of wave propagation at the localization-delocalization transition in the Harper equation (at $\epsilon=2$).

The Harper equation (9) possesses an evident symmetry, being invariant with respect to the spatial reflection $n\to-n$. Hence it is possible to construct a symmetric solution. For this we have to set $\psi_1=\psi_{-1}=[1-(b+\epsilon)/2]\psi_0$. According to Eq. (8), the corresponding orbit of the fractional-linear map (3) has an initial condition

$$x_0=(b+\epsilon)/(b+\epsilon-2). \tag{16}$$

If this orbit is localized (which occurs at one special value of b for each ϵ), it will correspond to the situation of the attractor-repeller collision. This is also true for periodic orbits corresponding to rational approximants w_k at $u=0$ [see Eq. (4)], and this notion is technically useful for computation of the sequence of parameter b values converging to the critical point TF (Sec. III).

V. RENORMALIZATION GROUP ANALYSIS

Let us develop now the RG approach to the dynamics at the TF critical point. Here we prefer to write out the original model in the form of a two-dimensional mapping

$$x_{n+1}=x_n/(1-x_n)+b+\epsilon\cos(2\pi u_n),$$
$$u_{n+1}=u_n+w \bmod 1, \tag{17}$$

and assume, for convenience, that the phase variable u is defined in such a way that it always belongs to the interval $(-0.5,0.5)$.

As the frequency parameter is the inverse golden mean, it is natural to deal with the evolution operators corresponding to Fibonacci's numbers of iterations.

We need to introduce here a new variable X (it differs from x by a u-dependent shift, but details will be explained below). Let $f^{F_k}(X,u)$ and $f^{F_{k+1}}(X,u)$ be the functions rep-

resenting transformation of X after F_k and F_{k+1} iterations, respectively. To construct the next operator, for F_{k+2} steps, we start from (X,u) and perform first the F_{k+1} iteration to arrive at $(f^{F_{k+1}}(X,u), \quad u+F_{k+1}w)$, and then the remaining F_k iterations with the result

$$f^{F_{k+2}}(X,u)=f^{F_k}(f^{F_{k+1}}(X,u),\ u+wF_{k+1}). \tag{18}$$

To have a reasonable limit behavior of the sequence of evolution operators we change scales for X and u by some appropriate factors α and β at each step of the construction, and define the renormalized functions as

$$g_k(X,u)=\alpha^k f(X/\alpha^k,\ (-w)^k u). \tag{19}$$

Note that $wF_{k+1}=-(-w)^{k+1}(\mathrm{mod}\,1)$, so it is natural to set $\beta=-1/w$. Rewriting Eq. (18) in terms of the renormalized functions we come to the functional equation

$$g_{k+2}(X,u)=\alpha^2 g_k(\alpha^{-1}g_{k+1}(X/\alpha,-wu),w^2u+w). \tag{20}$$

The same equation was obtained in the RG analysis of the critical points TDT (torus doubling terminal) and TCT (torus collision terminal) [15,16]. Here we will deal with another solution of that equation, associated with the TF (torus fractalization) critical point. To find out of what kind this solution is, we may attempt to compute the functions g_k from direct iterations of the map (17).

As mentioned, the variable x in the original map must be distinguished from X used in the derivation of the RG equation. In other words, we have to produce a variable change to pass to an appropriate ''scaling coordinate system'' in the two-dimensional phase space (u,x). The new coordinates may be defined as

$$X\propto x-x_c+Pu+Qu^2, \quad U=u, \tag{21}$$

where x_c is obtained from Eq. (16) with the substitutions $\epsilon=\epsilon_c=2$, $b=b_c$; P, and Q are some coefficients.

To evaluate the coefficients P and Q we can act as follows. Let us perform iterations of the map (17) at the critical point $\epsilon=2, b=b_c$, starting from $u_0=0$ and $x_0=x_c$ [see Eq. (16)], and compute the values of u and x after F_k and F_{k+1} iterations. Let these be (u_{F_k},x_{F_k}) and $(u_{F_{k+1}},x_{F_{k+1}})$, respectively. Three points $(0,x_c)$, (u_{F_k},x_{F_k}), and $(u_{F_{k+1}},x_{F_{k+1}})$ determine a parabola on the (u,x) plane, and its equation is given by $x-x_c+Pu+Qu^2=0$. The coefficients may be easily evaluated from coordinates of the three points. Of course, the result will depend on the level number k, and we must estimate the asymptotical limits for the coefficients; they are $P=5.926\,67$ and $Q=-210.629$. (In fact, the convergence is rather slow, but it is possible to guess its character, and obtain sufficiently good estimates.)

Now the procedure consists of the following.

(1) Fix k and the corresponding F_k.

(2) For given X and U define the initial conditions for the map (17): $x=XA\alpha^{-k}+x_c-PU-QU^2, \quad u=U$, where A is an arbitrary constant, $\beta=-1/w$, and $\alpha=2.89$ (this value has been selected in the course of computations as the most appropriate one).

(3) Produce F_k iterations of the map (17).

(4) Return to the variables (X,U) by the inverse change $X=\alpha^k A^{-1}(x_{F_k}-x_c+Pu_{F_k}+Qu_{F_k}^2), \quad U=u_{F_k}$.

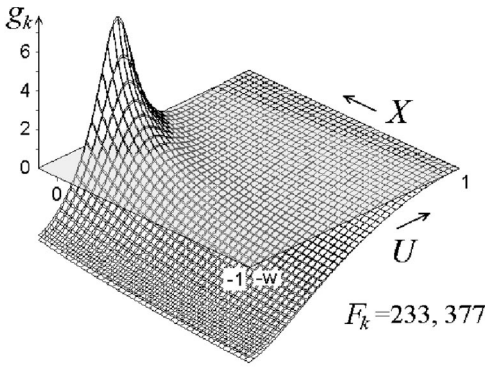

FIG. 6. 3D plots for the functions obtained from direct iterations of the fractional-linear map at $\epsilon=2$, $b=b_c=-0.597\,515\ldots$ with appropriate renormalization as explained in the text (the arbitrary constant mentioned in the text is chosen as $A=84$). The number of iterations $F_k=233$ and 377. Coincidence of both plots indicates that the functions approach the fixed point of the RG transformation.

Figure 6 presents graphically a sample of the results of such computations for two Fibonacci numbers $F_k=233$ and 377. The 3D plots of the two functions obtained are superimposed; observe their excellent agreement. (A yet better degree of coincidence was found for larger Fibonacci numbers.) This is an indication that we are dealing with a fixed-point solution of the functional equation

$$g(X,u)=\alpha^2 g(\alpha^{-1}g(X/\alpha,-wu),\ w^2u+w). \tag{22}$$

Now it is worth emphasizing that the maps determining evolution over the Fibonacci numbers of iterations are constructed by a repetitive application of the fractional-linear mappings, and hence must relate to the same fractional-linear class. This implies that we may search for a solution of Eq. (20) in the form

$$g_k(X,u)=\frac{a_k(u)X+b_k(u)}{c_k(u)X+d_k(u)}, \tag{23}$$

where the coefficients a,b,c,d are some functions of u. Without loss of generality we may require them to satisfy the additional condition (''unimodularity'')

$$a_k(u)d_k(u)-b_k(u)c_k(u)\equiv 1, \tag{24}$$

and set, as convenient, $c_k(0)=-1$. Substituting Eq. (23) into Eq. (20) we arrive at the RG equation reformulated in terms of the coefficients:

TABLE II. The polynomial coefficients for the fixed-point solution of the RG equation.

	$a(u)$	$b(u)$	$c(u)$	$d(u)$
1	3.180070169	0.329861441	-1.000000000	0.210730746
u	-3.450688327	-0.003027254	-0.601533776	0.167219763
u^2	-3.247090086	-8.330520346	0.443802007	3.062831633
u^3	3.992032627	9.444480715	0.293604279	1.865595582
u^4	1.200194704	11.133767028	-0.094027530	-1.597931152
u^5	-1.549680177	-13.205541847	-0.058193081	-1.044745269
u^6	-0.187890799	-4.313300571	0.011160724	0.358377518
u^7	0.286983991	5.592822816	0.006427031	0.223393531
u^8	0.016720852	0.734433497	-0.000847235	-0.044603872
u^9	-0.031115111	-1.104258820	-0.000457454	-0.025974096
u^{10}	-0.000950352	-0.069739548	0.000044648	0.003533563
u^{11}	0.002215271	0.125757870	0.000022730	0.001923598
u^{12}	0.000035770	0.004131194	-0.000001582	-0.000192702
u^{13}	-0.000110612	-0.009312156	-0.000000761	-0.000098574
u^{14}	-0.000000838	-0.000160051		0.000006910
u^{15}	0.000003663	0.000479736		0.000003335
u^{16}		0.000003822		
u^{17}		-0.000016158		

$$\begin{pmatrix} a_{k+2}(u) & b_{k+2}(u) \\ c_{k+2}(u) & d_{k+2}(u) \end{pmatrix} = \begin{pmatrix} a_k(w^2u+w) & \alpha^2 b_k(w^2u+w) \\ c_k(w^2u+w)/\alpha^2 & d_k(w^2u+w) \end{pmatrix} \times \begin{pmatrix} a_{k+1}(-wu) & \alpha b_{k+1}(-wu) \\ c_{k+1}(-wu)/\alpha & d_{k+1}(-wu) \end{pmatrix}. \quad (25)$$

To find the fixed point of this functional equation numerically we approximate the functions $a(u)$, $b(u)$, $c(u)$, and $d(u)$ by finite polynomial expansions. [Actually, the representation via Chebyshev's polynomials on an interval $u \in (-1,1)$ has been used.] Then, we organize the RG transformation as a computer program, which calculates the set of expansion coefficients for the functions $a_{k+2}(u), b_{k+2}(u), c_{k+2}(u)$ from two previous sets, $a_{k+1}(u), b_{k+1}(u), c_{k+1}(u)$ and $a_k(u), b_k(u), c_k(u)$. (Note that, due to the unimodularity, only three of the four functions are independent.) The fixed-point conditions are

$$(a_{k+2},\ b_{k+2},\ c_{k+2}) = (a_{k+1},\ b_{k+1},\ c_{k+1})$$

and

$$(a_{k+1},\ b_{k+1},\ c_{k+1}) = (a_k,\ b_k,\ c_k). \quad (26)$$

In terms of the polynomial representation this is equivalent to some finite set of algebraic equations with respect to the unknown coefficients of the polynomials and the unknown constant α. This problem was solved by means of the multidimensional Newton method. As an initial guess, a function obtained from iterations of the original map (see Fig. 6) was used. The resulting coefficients for the functions $a(u)$, $b(u)$, $c(u)$, and $d(u)$ corresponding to the fixed point are presented in Table II, and graphically in Fig. 7(a). Figure 7(b) shows a 3D plot of the fixed-point function; it may be compared with Fig. 6. The constant α that is the scaling factor for the X variable is found to be

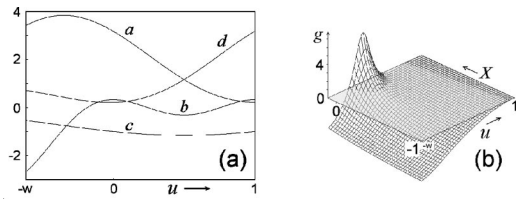

FIG. 7. Coefficients for the fixed-point fractional-linear solution of the RG equation versus phase variable u (a) and 3D plot of the universal function (b).

$$\alpha = 2.890\,053\,525\ldots, \quad (27)$$

in good agreement with the previously mentioned empirical estimate $\simeq 2.89$.

It is worth mentioning one more universal constant associated with the critical point. Evaluating the derivative of $g(X,u) = (a(u)X + b(u))/(c(u)X + d(u))$ with respect to X at the origin yields $\gamma = [\partial g(X,u)/\partial X]_{X=0,\,u=0} = 1/d(0)^2 = 22.518\,745\ldots$. As $g(X,u)$ represents the asymptotic form of the evolution operator for Fibonacci numbers of iterations, and X differs from x only by the u-dependent shift, we conclude that the constant γ will appear as the asymptotic value of the derivative $\partial x_{F_k}/\partial x_0$ if x_0 is selected in accordance with Eq. (17).

This gives the foundation for a method of locating the critical point. One composes a program to iterate the original map together with the recursive computation of $\partial x_n/\partial x_0$, and tries to select an appropriate value of b to obtain $\partial x_{F_k}/\partial x_0 = \gamma$. The result quickly converges to the critical point b_c as k grows. This method appears to be the most accurate, and the best numerical data [see Eq. (5)] have been obtained with its help.

VI. SCALING PROPERTIES OF DYNAMICS AT THE CRITICAL POINT

Let us consider an attractor at the critical point of our model map (17). Its portrait is shown in left panel of Fig. 8 in

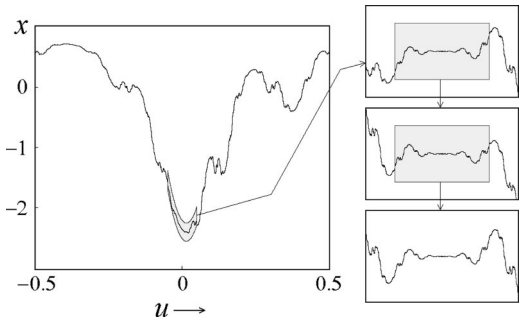

FIG. 8. Portrait of the critical attractor in natural variables $u_n = nw + u, x_n$ (left panel) and fragments of the picture shown under subsequent magnification in the curvilinear "scaling coordinate" system. At each step the magnification is increased by a factor $\alpha = 2.890\,05\ldots$ along the vertical axis and $\beta = -1.618\,03\ldots$ along the horizontal axis.

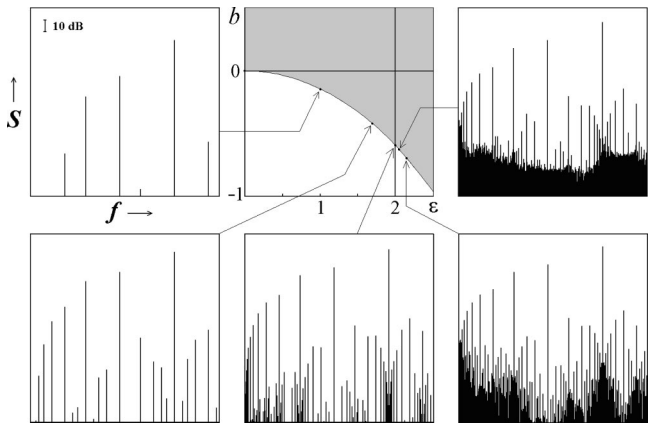

FIG. 9. Evolution of Fourier spectra generated by the map (3) along the bifurcation curve that corresponds to a threshold of intermittency.

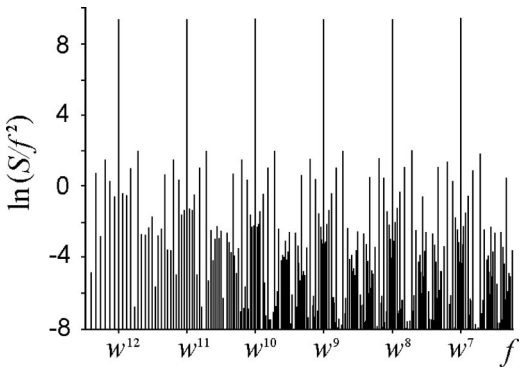

FIG. 10. Fourier spectrum at the TF critical point presented on a double logarithmic scale. Notice visible repetition of the structure in respect to a shift along the frequency axis.

natural variables (u_n, x_n). Depicting a part of the plot in "scaling coordinates" (U,X) we reveal a scaling property intrinsic to the attractor: The structure is reproduced again and again at each subsequent step of magnification by the factors α and β along the vertical and horizontal axes, respectively. This scaling property follows directly from the fact that in scaling coordinates the evolution operators for different Fibonacci numbers of iterations are asymptotically the same, up to the scale change (recall Fig. 6).

From the scaling property one can deduce an asymptotic expression for the form of the invariant curve at small scales near the origin. The form reproduces itself under simultaneous scale change by the factors α and $\beta=-1/w$ along the axes X and U, respectively, so it must behave locally as $X \propto |U|^{\kappa}$ with $\kappa=\ln\alpha/\ln|\beta|\approx 2.2054$. It follows that this is a smooth curve, twice differentiable at the origin, but the third derivative diverges. Due to the ergodicity ensured by irrationality of the frequency, the weak singularity at the origin implies the existence of the same type of singularities over the whole invariant curve, on a dense set of points. Apparently, the observed wrinkled form of the invariant curve at the critical point (see Figs. 2 and 8) reflects the presence of the mentioned set of dense weak singularities.

Figure 9 shows the evolution of the Fourier spectra generated by the map (17) as we move in the parameter plane along the bifurcation curve that corresponds to a threshold of intermittency. These spectra may be useful for comparison with possible experimental studies of the transition. For small ϵ, i.e., far enough from the critical value, the spectrum contains a few components. It is enriched by many additional lines at intermediate frequencies as we come to the critical or supercritical values of ϵ. At the critical point the spectrum has a self-similar structure. It can be revealed by the use of the double logarithmic scale (as suggested in a different context in Refs. [10–12]); see Fig. 10.

VII. LINEARIZED RG EQUATION AND SPECTRUM OF EIGENVALUES

A shift of parameters in the map (17) from the critical point corresponds to some perturbation of the evolution operator, and this perturbation will evolve under subsequent application of the RG transformation (20). Let us assume that the perturbation retains our evolution operators in the class of fractional-linear mappings. This means that we can search for a solution of Eq. (20) in the form

$$g_k(X,u)=\frac{(a_k(u)+\tilde{a}_k(u))X+b_k(u)+\tilde{b}_k(u)}{(c_k(u)+\tilde{c}_k(u))X+d_k(u)+\tilde{d}_k(u)}, \qquad (28)$$

where $a(u)$, $b(u)$, $c(u)$, and $d(u)$ correspond to the fixed-point solution, while the terms with a tilde are responsible for the perturbation. Then the substitution $(\tilde{a}_k(u),\ \tilde{b}_k(u),\ \tilde{c}_k(u),\ \tilde{d}_k(u)) \propto \delta^k$ gives rise to the eigenvalue problem

$$\delta^2\begin{pmatrix}\tilde{a}(u) & \tilde{b}(u)\\ \tilde{c}(u) & \tilde{d}(u)\end{pmatrix}=\delta\begin{pmatrix}a(w^2u+w) & \alpha^2 b(w^2u+w)\\ c(w^2u+w)/\alpha^2 & d(w^2u+w)\end{pmatrix}\begin{pmatrix}\tilde{a}(-wu) & \alpha\tilde{b}(-wu)\\ \tilde{c}(-wu)/\alpha & \tilde{d}(-wu)\end{pmatrix}$$
$$+\begin{pmatrix}\tilde{a}(w^2u+w) & \alpha^2\tilde{b}(w^2u+w)\\ \tilde{c}(w^2u+w)/\alpha^2 & \tilde{d}(w^2u+w)\end{pmatrix}\begin{pmatrix}a(-wu) & \alpha b(-wu)\\ c(-wu)/\alpha & d(-wu)\end{pmatrix}. \qquad (29)$$

As usual, only the eigenvalues larger than 1 in modulus are of interest because the corresponding perturbations grow under repetition of the RG transformation and hence may influence the form of the long-time evolution operators.

TABLE III. The eigenvalues larger than or equal to 1 in modulus.

Eigenvalue	Designation	Interpretation
3.134272989	δ_1	Relevant eigenvalue
-2.890053625	$-\alpha$	Noncommutative subspace
2.890053625	α	The variable change $x \leftarrow x+\varepsilon$
-1.786151370	$-\alpha w^{-1}$	The variable change $x \leftarrow x+\varepsilon u$
1.786151370	αw^{-1}	Noncommutative subspace
-1.618033979	$-w^{-1}$	The variable change $u \leftarrow u+\varepsilon$
1.618033979	$\delta_2 = w^{-1}$	Relevant eigenvalue
1.618033979	w^{-1}	Violation of the unimodularity
1.103902257	αw^{-2}	The variable change $x \leftarrow x+\varepsilon u^2$
-1.103902257	$-\alpha w^{-2}$	Noncommutative subspace
1.000000000	1	The variable change $x \leftarrow x(1+\varepsilon)$
-1.000000000	-1	Noncommutative subspace
-1.000000000	-1	Noncommutative subspace

Numerically, we solved the problem by use of finite polynomial approximations for the functions involved, taking into account the previously found fixed-point solution. Equation (29) then gives rise to an eigenvalue problem defined in terms of finite-dimensional matrices acting in a vector space of coefficients for the polynomial expansions of the functions $\tilde{a}(u)$, $\tilde{b}(u)$, $\tilde{c}(u)$, and $\tilde{d}(u)$, and it can be dealt with by standard methods of linear algebra. The computations reveal 13 eigenvalues larger than or equal to 1 in modulus; they are listed in Table III.

Actually, only a few of them are of relevance. First, some of the eigenvectors found are associated with infinitesimal variable changes. For example, with a substitution $X \to X+\varepsilon$ in the map (23) we arrive at the new map

$$X_{n+1} = \frac{a(u)X_n + \varepsilon a(u) + b(u)}{c(u)X_n + \varepsilon c(u) + d(u)} - \varepsilon. \tag{30}$$

The right-hand part is represented in the first order in ε as

$$g(X,u) + \tilde{g}(X,u) \cong \frac{(a(u)+\tilde{a}(u))X_n + (b(u)+\tilde{b}(u))}{(c(u)+\tilde{c}(u))X_n + (d(u)+\tilde{d}(u))}, \tag{31}$$

where $(\tilde{a}(u),\tilde{b}(u),\tilde{c}(u),\tilde{d}(u)) = \varepsilon(1-c(u),-d(u),1,0)$. In the course of the RG transformation X is rescaled as $X \to X/\alpha$, and the renormalized relative coordinate shift is multiplied by α too. So $(1-c(u),-d(u),1,0)$ represents an eigenvector, and α is the associated eigenvalue. [One can verify it by a direct substitution of the eigenvector into Eq. (29); moreover, the assertion has been checked also by accurate comparison of the present eigenvector components with those found numerically as functions of u.] So we may exclude the eigenvalue α from the list, because a perturbation of this kind in the evolution operator can always be compensated by a shift of the origin. In the same way, we regard several other eigenvectors as irrelevant; they are marked in Table III as linked with variable changes.

Second, in the derivation of the RG equation we have used a definite order for the evolution operators (first F_{k+1}, then F_k steps). However, this order may be inverted, and it leads to a distinct alternative formulation of the eigenvalue problem, namely,

$$\delta^2 \begin{pmatrix} \tilde{a}(u) & \tilde{b}(u) \\ \tilde{c}(u) & \tilde{d}(u) \end{pmatrix} = \delta \begin{pmatrix} \tilde{a}(-wu+w^{-1}) & \alpha\tilde{b}(-wu+w^{-1}) \\ \tilde{c}(-wu+w^{-1})/\alpha & \tilde{d}(-wu+w^{-1}) \end{pmatrix} \begin{pmatrix} a(w^2u) & \alpha^2 b(w^2u) \\ c(w^2u)/\alpha^2 & d(w^2u) \end{pmatrix} + \begin{pmatrix} a(-wu+w^{-1}) & \alpha b(-wu+w^{-1}) \\ c(-wu+w^{-1})/\alpha & d(-wu+w^{-1}) \end{pmatrix} \begin{pmatrix} \tilde{a}(w^2u) & \alpha^2\tilde{b}(w^2u) \\ \tilde{c}(w^2u)/\alpha^2 & \tilde{d}(w^2u) \end{pmatrix}. \tag{32}$$

The true evolution operators are in any case multiple compositions of the same original map. Thus, for the actual perturbations Eqs. (29) and (32) must be equivalent. In other words, only those eigenvectors can be of relevance, that are common to both the eigenvalue problems. This property was verified numerically for all the eigenvectors found. As observed, some of them do not satisfy the condition; in Table III they are marked as relating to a noncommutative subspace.

The remaining two eigenvalues

$$\delta_1 = 3.134\,272\,989\ldots$$

and

$$\delta_2 = w^{-1} = 1.618\,033\,979\ldots \tag{33}$$

are relevant and responsible for the scaling properties of the parameter space near the TF critical point.

If we depart from the critical point in the parameter plane along the bifurcation curve of the attractor-repeller collision,

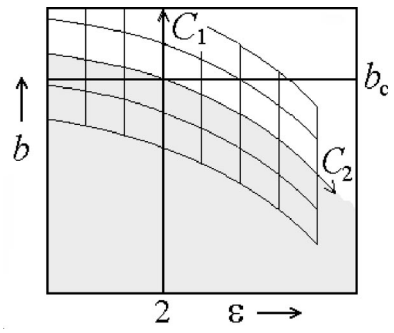

FIG. 11. Local coordinates on the parameter plane of the fractional-linear map appropriate for demonstrating scaling.

the first eigenvector appears not to contribute to the perturbation of the evolution operator. In this case the only relevant perturbation is associated with δ_2. However, if we choose a transversal direction, say, along the axis b, a perturbation of the first kind appears. This means that a coordinate system appropriate for observation of scaling in the parameter plane has to be defined as shown in Fig. 11. It is a curvilinear system: one coordinate axis is the line $\epsilon=2$, but the other follows the bifurcation border, accounting for its curvature. In the analytical expression it is sufficient to keep terms up to the second order. (This is due to the concrete relation between δ_1 and δ_2: $\delta_1>\delta_2$ and $\delta_1>\delta_2^2$, but $\delta_1<\delta_2^3$; see other examples of scaling coordinates for different critical points and discussion of the role of the relation of the eigenvalues in Refs. [13,16,30,31].)

So we set

$$b=b_c+C_1+pC_2+qC_2^2,$$

$$\epsilon=2+C_2, \tag{34}$$

where

$$p=(2-b_c)/4\cong -0.649\,38, \quad q\cong -0.336\,92. \tag{35}$$

The expression for p follows from the analogy with the Harper equation and from the Aubry transformation rule (15): An infinitesimal shift of ϵ and b along the tangent line to the bifurcation border must correspond to a shift of ϵ' and b' along the same line. The value of q is calculated numerically, from the curvature of the bifurcation border.

In addition to the obtained nontrivial solution of the RG equation there exists also a trivial, phase-independent fixed point

$$g(X,u)\equiv g(X)=X/(1-X), \tag{36}$$

with $\alpha=1/w=1.618\,034\ldots$. Naturally, this is the fixed point responsible for the behavior on the subcritical part of the bifurcation border and associated with the transition accompanied by a collision of smooth invariant curves. The eigenvalue problem for the linearized RG equation may be solved analytically for this case, and it reveals a unique relevant eigenvalue $\delta=1/w^2=2.618\,034\ldots$.

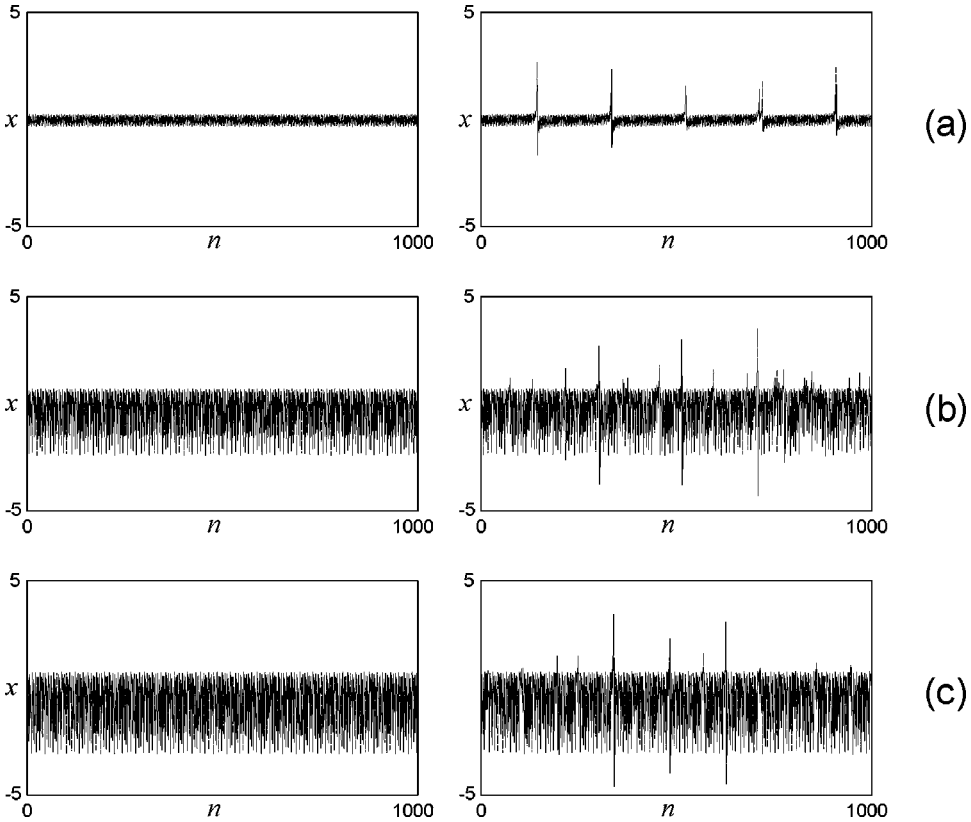

FIG. 12. The dynamical variable versus time in the model map (1) just before and after the transition: (a) a subcritical amplitude of driving, $\epsilon=0.5$; (b) the critical case, $\epsilon=2$; (c) a supercritical case, $\epsilon=2.3$.

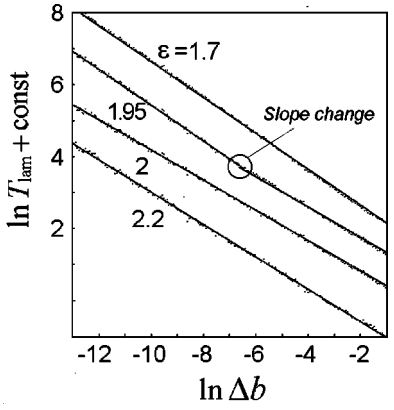

FIG. 13. Data from numerical experiments with the fractional-linear map: average duration of passage through the ''channel'' versus deflection from the bifurcation threshold for several values of ϵ on a double logarithmic scale. Observe the crossover phenomenon, the slope change from a critical to a subcritical value at some intermediate value of Δb for $\epsilon=1.95$.

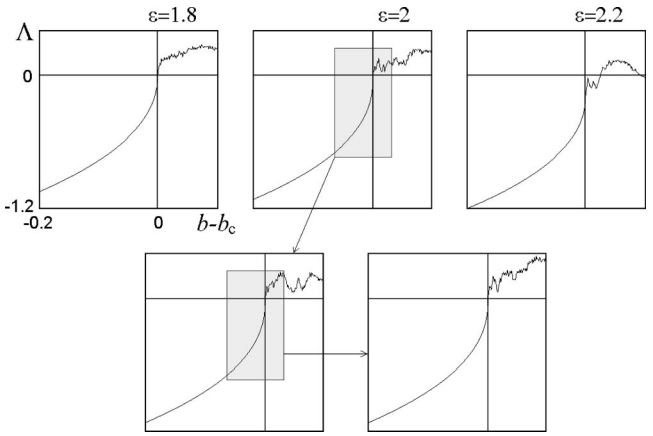

FIG. 14. Lyapunov exponent versus parameter b for subcritical, critical, and supercritical constant values of ϵ in the map (1). Illustration of scaling for the critical case: insets are shown with consecutive magnification by $\delta_1=3.134\,27\ldots$ along the horizontal axis, and by a factor $\theta=1.618\,03\ldots$ (the rescaling factor for time) along the vertical axis.

VIII. DYNAMICS IN A NEIGHBORHOOD OF THE CRITICAL POINT AND INTERMITTENCY

Let us discuss now the question of the peculiarities of intermittency in the quasiperiodically forced map. First of all, we outline the possibility of three distinct regimes at the onset of intermittency: the subcritical, $\epsilon<\epsilon_c=2$, when collision with coincidence of the smooth invariant curves (attractor and repeller) takes place at the moment of bifurcation; the critical, $\epsilon=\epsilon_c$, which corresponds to collision and coincidence of the wrinkled invariant curves (the threshold of fractalization); and the supercritical, $\epsilon>\epsilon_c$, where collision of the invariant curves occurs at some fractal subset of points.

Figures 12(a)–12(c) show the time dependencies for the dynamical variable generated by the model map (1) just before and after the transition for the three cases mentioned. In the intermittent regimes the ''laminar stages'' are interrupted by ''turbulent bursts.'' The laminar stages in the right panels reproduce approximately the patterns of the left panels.

The relative duration of the laminar phases becomes larger as we approach the transition point. In the usual Pomeau-Manneville intermittency of type I the average duration of the laminar stages behaves as

$$t_{\rm lam}\propto 1/|\Delta b|^{\nu} \tag{37}$$

TABLE IV. Comparison of the numerical results and RG predictions for the critical exponent.

ε	ν, numerics	ν, theory
1.7	0.508	0.5
2.0	0.424	0.42123
2.2	0.452	?
2.3	0.456	?

with $\nu=0.5$ [17–19].

In the presence of a quasiperiodic force the same law is valid in the subcritical region $\epsilon<2$. In the critical case $\epsilon=2$ the exponent is distinct. Indeed, as follows from the RG results, to observe an increase of the characteristic time scale by a factor $\theta=1/w=1.618\,03\ldots$ we have to decrease the shift of the parameter b from the bifurcation threshold by a factor $\delta_1=3.134\,27\ldots$. It follows that the exponent must be

$$\nu=\ln\theta/\ln\delta_1\cong 0.421\,23. \tag{38}$$

[Note that substitution of the δ factor associated with the trivial fixed point (36) yields just the result for the subcritical region, $\nu=0.5$.]

Figure 13 shows the data for numerical experiments with the fractional-linear map aimed at verifying the theoretical predictions for the exponent ν. At each fixed ϵ we empiri-

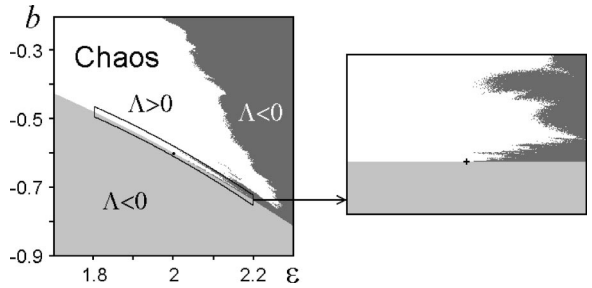

FIG. 15. A chart of the parameter plane or the ''phase diagram'' in natural variables (left panel) and in scaling coordinates (right panel). The gray areas correspond to negative Lyapunov exponent values, with distinct tones for localized attractors (smooth tori) in the bottom area, and to intermittent regimes associated presumably with a SNA in the top area to the right.

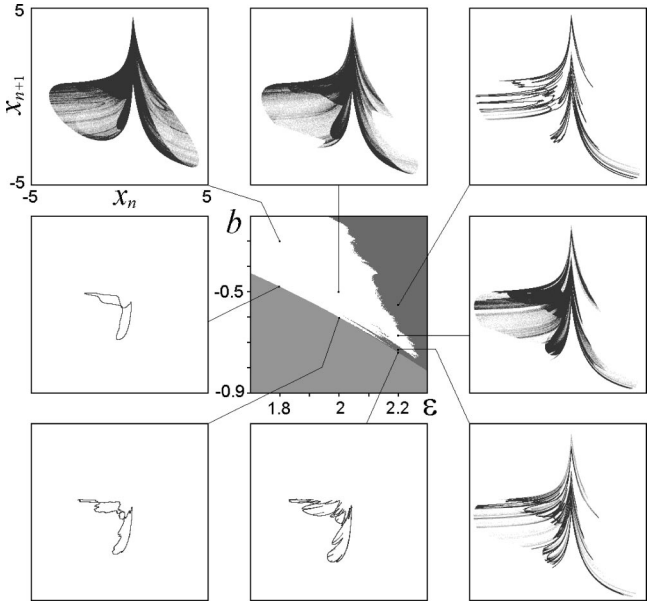

FIG. 16. Portraits of attractors at several representative points of the phase diagram.

cally determined the average duration of passage through the ''channel'' in dependence on Δb for an ensemble of orbits with random initial conditions, and plotted the results on a double logarithmic scale. For particular $\epsilon=1.7$ (subcritical) and 2 (critical) the dependencies fit straight lines of definite slope. As seen from Table IV, the correspondence of the numerical results with the theoretical predictions is rather good. At subcritical ϵ slightly less than 2 one can observe a crossover phenomenon, that is, the slope changes from a critical to a subcritical value at some intermediate value of Δb.

It is interesting that the results obtained for the supercritical region also indicate a constant definite slope, $\nu\approx 0.45$. At this moment it is not clear how to explain this observation theoretically.

Figure 14 shows diagrams for the Lyapunov exponents versus the parameter b for subcritical, critical, and supercritical constant values of ϵ in the artificial map (1), which includes the reinjection mechanism.

For the subcritical case the intermittency threshold corresponds to the onset of chaos: The Lyapunov exponent becomes positive immediately after the transition.

In the supercritical region the Lyapunov exponent is still negative at the moment of the bifurcation; it cannot immediately become positive, and the transition will be accompanied by creation of a SNA rather than a chaotic attractor.

In the critical situation the diagram demonstrates self-similarity (at least, in the domain $b<b_c$): Magnification by the factor $\delta_1=3.134\,27\ldots$ along the horizontal axis, and by the factor $\theta=1.618\,03\ldots$ (the rescaling factor for time) along the vertical axis gives rise to similar pictures.

Figure 15 demonstrates a chart of the parameter plane, or the ''phase diagram'' in the natural variables (left panel) and in the scaling coordinates (right panel). The gray areas are those of negative Lyapunov exponent; the two distinct tones correspond to the domains of existence of the localized attractors (smooth tori in the bottom area) and the intermittent regimes (the top area to the right). Apparently, the last is the region of the SNA. This assertion may be deduced from the arguments of Pikovsky and Feudel [6]. Indeed, considering the dynamics there in terms of rational approximants one can notice that phase-dependent bifurcations will occur inevitably. In contrast, the white area of positive Lyapunov exponent is the domain of chaotic intermittent regimes. Figure 16 shows portraits of attractors at several representative points of the phase diagram.

IX. CONCLUSION

The present study was devoted to one special situation of transition from conventional quasiperiodicity (''smooth torus'') to chaos or the SNA via intermittency in a model map under quasiperiodic external driving with the frequency parameter defined as the inverse golden mean. The main attention was concentrated on the critical situation reached at one particular, sufficiently large amplitude of driving, associated with the threshold of fractalization. Here a bifurcation transition analogous to the tangent bifurcation consists of a collision with the coincidence and subsequent disappearance of an attractor and a repeller represented by a pair of wrinkled invariant curves. An RG analysis appropriate for the critical situation was developed, the fixed-point solution of the RG equation was found in a class of fractional-linear functions, and the constants responsible for scaling in phase space and parameter space were computed.

Some related problems yet remain open; for example, concerning global scaling properties and dimensions of the critical attractor. Also a generalization for other irrational rotational numbers is of interest. (The last seems undoubtedly possible because of the analogy with the Harper equation: there the criticality at $\epsilon=2$ occurs at arbitrary values of the rotational number.) One more problem is the developement of an appropriate approach to analysis of the transition in the supercritical region, which would be of the same significance as is the RG method in the critical and subcritical cases.

As is common in situations allowing RG analysis, one can expect that the quantitative regularities intrinsic to our model map will be valid also in other systems relating to the same universality class. In particular, it may be suggested that the transition to the SNA observed in a quasiperiodically forced subcritical circle map [28] is of the same nature. Also, it would be significant to find this type of behavior in systems of higher dimension, for example, in quasiperiodically driven invertible 2D maps, which could represent the Poincaré maps of some flow systems.

It would be interesting to reveal the details and regularities of the coexistence (subordination) of the type of critical behavior discussed here with the behaviors of the distinct universality classes studied in Refs. [14–16] (e.g., the torus-collision terminal and torus-doubling terminal points).

ACKNOWLEDGMENTS

The work was supported by RFBR Grant No. 00-02-17509. The appearance of this work was stimulated by discussions with Arkady Pikovsky and Eireen Neumann during the workshop ''Statistical Mechanics of Space-Time Chaos'' organized by the Max Planck Institute of Physics of Complex Systems. I thank Igor Sataev for valuable help in numerical solution of the RG equation and associated eigenvalue problem, and Andrew Osbaldestin for discussions during my visit to Loughborough University.

[1] L. D. Landau, C. R. (Dokl.) Acad. Sci. URSS **44**, 311 (1944).
[2] E. Hopf, Commun. Pure Appl. Math. **1**, 303 (1948).
[3] D. Ruelle and F. Takens, Commun. Math. Phys. **20**, 167 (1971).
[4] C. Grebogi, E. Ott, S. Pelikan, and J. A. Yorke, Physica D **13**, 261 (1984).
[5] F. J. Romeiras, A. Bondeson, E. Ott, T. M. Antonsen, and C. Grebogi, Physica D **26**, 277 (1987).
[6] A. S. Pikovsky and U. Feudel, Chaos **5**, 253 (1995).
[7] M. J. Feigenbaum, J. Stat. Phys. **19**, 25 (1978).
[8] M. J. Feigenbaum, J. Stat. Phys. **21**, 669 (1979).
[9] E. B. Vul, Y. G. Sinai, and K. M. Khanin, Russ. Math. Surveys **39**, 1 (1984).
[10] D. Rand, S. Ostlund, J. Sethna, and E. D. Siggia, Phys. Rev. Lett. **49**, 132 (1982).
[11] S. Ostlund, D. Rand, J. Sethna, and E. D. Siggia, Physica D **8**, 303 (1983).
[12] M. J. Feigenbaum, L. P. Kadanoff, and S. J. Shenker, Physica D **5**, 370 (1982).
[13] A. P. Kuznetsov, S. P. Kuznetsov, and I. R. Sataev, Physica D **109**, 91 (1997).
[14] S. P. Kuznetsov, A. S. Pikovsky, and U. Feudel, Phys. Rev. E **51**, R1629 (1995).
[15] S. Kuznetsov, U. Feudel, and A. Pikovsky, Phys. Rev. E **57**, 1585 (1998).
[16] S. P. Kuznetsov, E. Neumann, A. Pikovsky, and I. R. Sataev, Phys. Rev. E **62**, 1995 (2000).
[17] Y. Pomeau and P. Manneville, Commun. Math. Phys. **74**, 189 (1980).
[18] B. Hu and J. Rudnick, Phys. Rev. Lett. **48**, 1645 (1982).
[19] J. E. Hirsch, B. A. Huberman, and D. J. Scalapino, Phys. Rev. A **25**, 519 (1982).
[20] F. Argoul and A. Arneodo, J. Phys. (France) **46**, L901 (1985); H. Daido, Prog. Theor. Phys. **71**, 402 (1984).
[21] U. Feudel, A. S. Pikovsky, and J. Kurths, Physica D **88**, 176 (1995).
[22] P. G. Harper, Proc. Phys. Soc., London, Sect. A **68**, 854 (1955).
[23] I. M. Suslov, Zh. Eksp. Teor. Fiz. **83**, 1079 (1982).
[24] S. Ostlund and R. Pandit, Phys. Rev. B **29**, 1394 (1984).
[25] J. A. Ketoja and I. I. Satija, Physica D **109**, 70 (1997).
[26] B. D. Mestel, A. H. Osbaldestin, and B. Winn, J. Math. Phys. **41**, 8304 (2000).
[27] S. S. Negi and R. Ramaswamy, Phys. Rev. E **64**, 045204 (2001).
[28] H. Osinga, J. Wiersig, P. Glendinning, and U. Feudel, Int. J. Bifurcation Chaos Appl. Sci. Eng. **11**, 3085 (2001).
[29] S. Aubry and G. Andre, in *Proceedings of the Israel Physical Society*, edited by C. G.Kuper (Hilger, Bristol, 1979), Vol. 3, p. 133.
[30] A. P. Kuznetsov, S. P. Kuznetsov, and I. R. Sataev, Phys. Lett. A **189**, 367 (1994).
[31] N. Y. Ivankov and S. P. Kuznetsov, Phys. Rev. E **63**, 046210 (2001).